2021 43rd Annual International Conference of the
IEEE Engineering in Medicine & Biology Society (EMBC)
Oct 31 - Nov 4, 2021. Virtual Conference

Identification of Motor Unit Twitch Properties in the Intact Human In Vivo

Antonio Gogeascoechea Hernandez, Rafael Ornelas Kobayashi, Utku S. Yavuz, and Massimo Sartori

Abstract— **Restoring natural motor function in neurologically injured individuals is challenging, largely due to the lack of personalization in current neurorehabilitation technologies. Signal-driven neuro-musculoskeletal models may offer a novel paradigm for devising novel closed-loop rehabilitation strategies according to an individual's physiology. However, current modelling techniques are constrained to bipolar electromyography (EMG), thereby lacking the resolution necessary to extract the activity of individual motor units (MUs) *in vivo*. In this work, we decoded MU spike trains from high-density (HD)-EMG to obtain relevant neural properties across multiple isometric plantar-dorsiflexion tasks. Then, we sampled MU statistical distributions and used them to reproduce MU specific activation profiles. Results showed bimodal distributions which may correspond to slow and fast MU populations. The estimated activation profiles showed a high degree of similarity to the reference torque (R^2>0.8) across the recorded muscles. This suggests that the estimation of MU twitch properties is a crucial step for the translation of neural information into muscle force.**

Clinical Relevance— **This work has multiple implications for understanding the underlying mechanism of motor impairment and for developing closed-loop strategies for modulating alpha motor circuitries in neurologically injured individuals.**

I. Introduction

The development of neuro-prostheses (*e.g.* spinal cord electrical stimulation and robotic exoskeletons) is currently hindered by our limited understanding of the interaction between neural and mechanical levels of human movement. As human motor function is highly variable across motor tasks and individuals [1]–[3], current neurorehabilitation technologies operate in open-loop and rely on empirical inspection. This prevents optimal restoration of motor function in neurologically injured patients.

Computational simulations of the neuro-musculoskeletal system help expand our knowledge of the underlying spinal mechanisms of healthy [4] and pathological [5] motor function. Moreover, personalized, signal-driven neuro-musculoskeletal models [6], [7] take one step further by not only representing force-generation processes, but also capturing the within and between-subject variability. However, such models are often driven by global electromyograms (EMGs) and hence, offer a limited representation of the excitation-contraction coupling. In this regard, the ability of decoding motor units (MU) from higher resolution EMG (*i.e.*, high-density [HD]-EMG) *in vivo* opens up new avenues to extend current activation dynamics formulations. Moreover, as the MUs are the quantum elements of the nervous system to generate movement, measuring their activity is crucial to develop rehabilitation technology for restoring lost motor function.

The access to motor neuron information enables the non-invasive identification and characterization of pathological neural patterns [8], [9]. In turn, this leads to investigating how spinal motor circuitries respond to electrical or mechanical stimuli (*i.e.*, response to neurorehabilitation devices). A recent study [10], for example, has shown how the strength of common synaptic input is altered by transcutaneous spinal electrical stimulation in spinal cord injured individuals. We aim at linking such *in vivo* approaches with the mechanical output through signal-driven neuro-musculoskeletal models. For this, the first step is to translate the language of the nervous system into muscle contractile properties.

This study presents our ongoing efforts to build relations between the neural and musculoskeletal levels of movement in the intact human *in vivo*. First, we propose a technique to sample MU distributions across multiple trials and levels of activation. Second, we employ such distributions to reproduce MU-specific activation dynamics. This may lead to the development of closed-loop control strategies for neuromodulation, thereby enhancing movement in an optimal manner.

II. Methods

A. Experimental procedures

Experiments were approved by the University Medical Center Göttingen Ethical Committee (Ethikkommission der Universitätsmedizin Göttingen, approval number 01/10/12). The detailed procedures are described elsewhere [11]. Briefly, we selected a subset of a healthy subject who performed isometric plantar-dorsiflexion contractions (Fig 1.A) across three initial positions: anatomical (0°), 10° plantar- and 10° dorsiflexed; across different levels of activation: ramp up to 30, 50, 70, and 90% of maximum voluntary contraction (MVC); and across fixed and variable slopes of activation. HD-EMGs were recorded using a 256-channel EMG amplifier (EMG-USB2, OT Bioelettronica, Torino, Italy) from the tibialis anterior, gastrocnemius, soleus, and peroneus (2048 Hz sampling frequency). The reference electrode was

* Research supported by the European Research Council Starting Grant INTERACT (grant no. 803035).

A. Gogeascoechea Hernandez, R. Ornelas Kobayashi and M. Sartori are with the Department of Biomechanical Engineering, University of Twente, Netherlands. (email: a.d.j.gogeascoecheahernandez@utwente.nl).

U. S. Yavuz is with the Biomedical Signals and Systems Group, University of Twente.

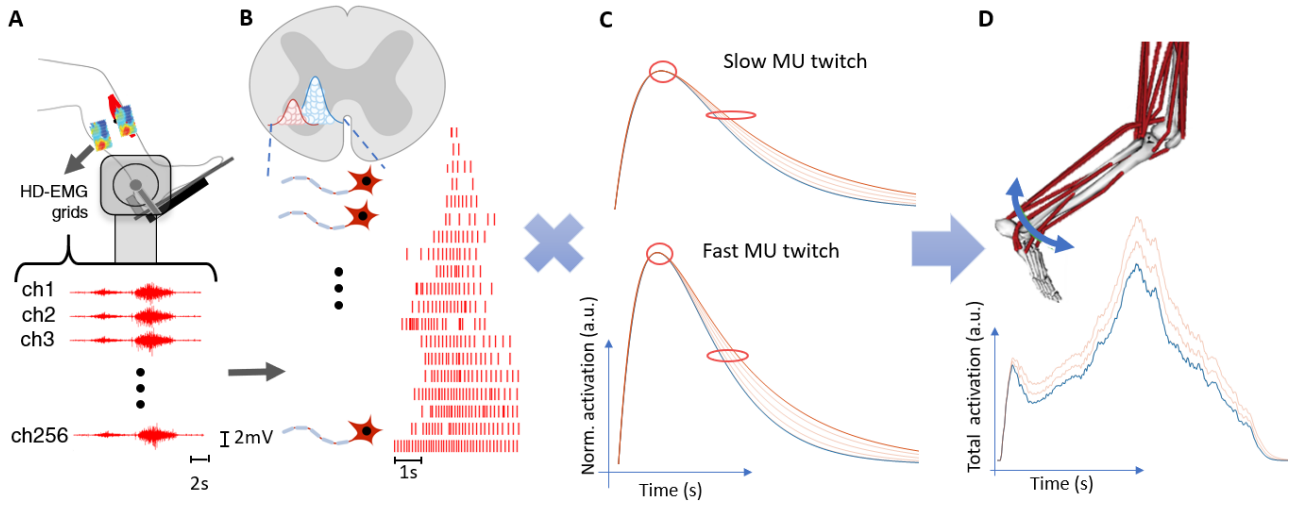

Figure 1. Overview of motor unit (MU)-specific activation dynamics formulation. (A) The subjects performed plantar-dorsiflexion contractions and 256 monopolar channels (ch) of high-density electromyography (HD-EMG) were recorded. (B) The processed HD-EMGs were decomposed into MU spike trains for each muscle. Thereafter, the mean discharge rate and recruitment threshold were computed for each MU. Finally, gaussian distributions were fitted resulting in two populations of MUs (slow and fast). (C) Each twitch was designed as an impulse response of a critically damped system with MU-specific contractile parameters (in red circles) (D) The convolution between the spike trains and their specific twitch response results in an activation profile.

placed on the malleolus. Torque was measured with a dynamometer (M3, Biodex Medical Systems Inc., Shirley, NY, USA).

B. Sampling Motor Unit Distributions

HD-EMG and torque data were offline processed using Matlab R2021a (The Mathworks Inc., Natick, MA, USA). HD-EMGs were band-pass filtered (10-500 Hz) with a second-order Butterworth filter. The filtered signals were then decomposed into constituent MU spike trains using a convolutive blind source separation technique [12] (Fig 1.B). Each spike train consists of a binary vector where '1' indicates a discharge event, and '0' a non-discharge event. We assessed the quality of the spike trains and removed the noise sources as proposed in our previous work [10]. This addressed current limitations with the decomposition algorithm and ensured that only physiologically correct MUs were included.

After quality selection, we computed the mean discharge rate and recruitment threshold for each MU spike train. The mean discharge rate (*DR*) was defined as the mean inverse difference of the time elapsed between consecutive spikes:

$$DR = \frac{1}{N-1}\sum_{i=2}^{N}\frac{1}{t_i - t_{i-1}}, \qquad (1)$$

where t_i is the time event of the i^{th} spike and N is the total number of spikes in a single train.

The recruitment threshold (*RT*) was defined as the mean percentage of maximum voluntary contraction given around the first discharge:

$$RT = \frac{1}{w}\sum_{n=t_1-w/2}^{t_1+w/2} m(n), \qquad (2)$$

where *m* is the percentage of MVC (*i.e.*, normalized torque) and *w* is a 300-sample window (~150 ms) surrounding the first spike event (t_1). This accounts for torque fluctuations due to noise. Moreover, we selected only time intervals during the ramps to prevent estimating the recruitment threshold from isolated (sudden) spikes during resting periods.

These features alone do not display a clear distinction of MU-types, *i.e.*, without further processing, it is more challenging to predict twitch properties. Hence, we estimated a linear combination (eigenvector) that yields the largest possible variance of the decomposed MU features (Fig. 2.A and 2.B). For this, we normalized the mean discharge rate to a maximum of 40 Hz. We then reduced the dimensionality by extracting the first principal component (using singular value decomposition) and projected the data onto the first eigenvector (Fig. 2.A). We computed histograms of the projection and their respective probability density function using a gaussian mixture model (Fig. 2.B).

C. Activation dynamics formulation

As we aim to characterize a twitch response with a high degree of adjustability, we focused on three main parameters: peak amplitude, contraction time (time-to-peak), and half relaxation time (Fig 1.C). We described an MU-specific twitch response (Fig 1.D) as proposed by Raikova et al. [13]. For this model, the total MU-specific activation is given by the sum of the individual twitch responses (Fig. 3).

Additionally, we assessed the model proposed by Fuglevand et al. [14]. Although this model does not account for the half relaxation time, its discretized version is computationally efficient [15] and two parameters may be sufficient to obtain accurate activation profiles.

We estimated the contractile parameters from literature[16], [17]. To map the probability distributions into contraction times, we selected characteristic landmarks (*e.g.* limits of the eigenvector, location of the two peaks, and location of the valley between peaks). We then extracted the same landmarks from the contraction time distribution [16]

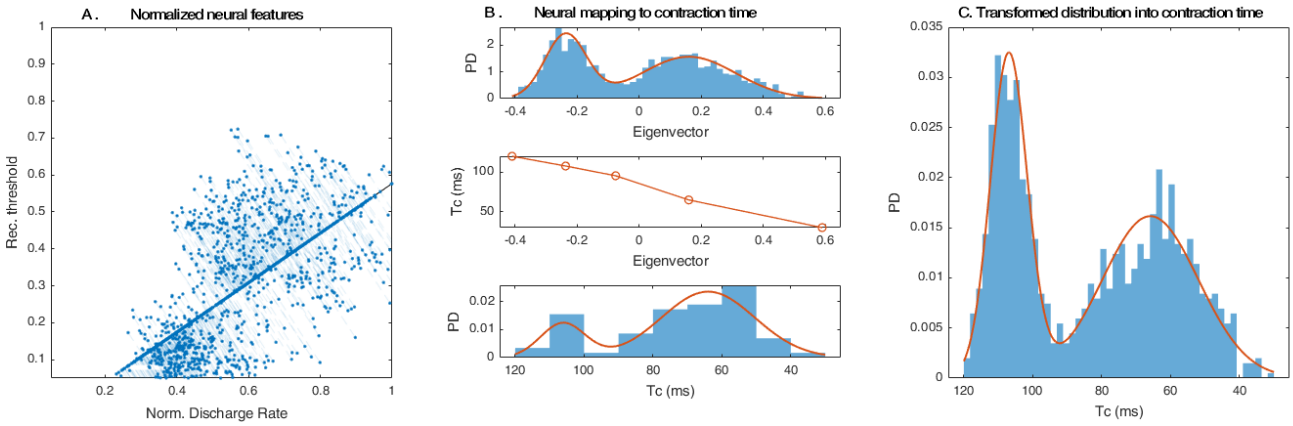

Figure 2. Neural mapping into twitch contraction time (tibialis anterior example). (A) Projection of normalized data onto the first principal component (eigenvector yielding the maximum variance of both features). Each point of the scatter plot represents a measurement (discharge rate and recruitment threshold) of a single motor unit (MU). (B) Histogram of data projection onto first eigenvector (top) and histogram of twitch contraction times measured in humans [16] (bottom). Both are normalized by the probability density function estimate, *i.e.*, by the total number of elements times the width of the bins. The mapping is achieved by piecewise linear interpolation (middle). (C) Resultant transformed distribution into twitch contraction times.

(Fig 2.B), and computed piecewise linear interpolation, thereby assigning a specific contraction time to each MU (Fig. 2.C). As the scope of this study is to investigate the shape of the activation profile, the twitch peak (amplitude) was set constant. Similarly, we assumed that the half relaxation time was approximately equal to the contraction time for Raikova's model [13]. This provides a faster twitch decay than the natural decay of Fuglevand's model [14], which is in line with experimental observations [16], [17].

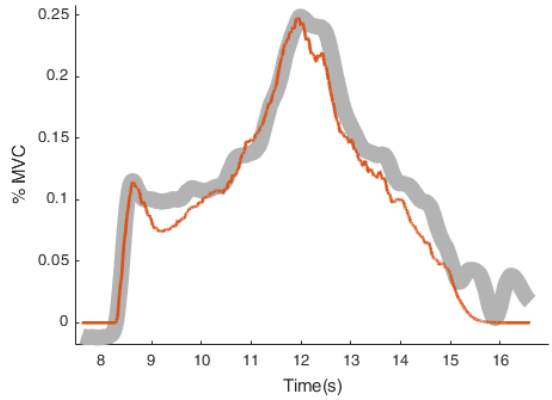

Figure 3. Example of activation profile (in red) from the tibialis anterior during a dorsiflexion task. The gray line corresponds to the normalized reference torque (% of maximum voluntary contraction [MVC])

III. Results

The projection of the neural features onto the first eigenvector resulted in bimodal distributions for all muscles (*e.g.,* tibialis anterior in Fig. 2.B). Namely, these projections contain information of two populations with slow and fast-twitch properties. The mean discharge rates and standard deviations of the two populations are displayed in table 1.

Fig. 4 depicts the coefficient of determination (R^2) between the reference torque and the estimated activation profiles for the twitch models. Both formulations tended to similar coefficients for most muscles: 0.92 for the tibialis anterior and the medial gastrocnemius, 0.83 for the soleus, and 0.88 for the lateral gastrocnemius. For the peroneus, the coefficients of determination slightly differed: 0.90 and 0.83 for Fuglevand's and Raikova's formulation, respectively. The majority of outliers (14 out of 16) corresponded to high-torque trials (*i.e.*, ramps up to 70% and 90% of MVC). Moreover, the computation time of Fuglevand's formulation was ~150 times shorter than Raikova's formulation.

TABLE I. Motor-unit Gaussian mixture means (and std.) of discharge rates (DR) and recruitment threshold (RT)

Muscles	***Slow (type I)***		***Fast (type IIa and IIb)***	
	DR (Hz)	***RT***	***DR***	***RT***
TA	16.3 (0.1)	0.11(0.003)	26.8(0.6)	0.41(0.017)
SOL	12.5(0.04)	0.10 (0.003)	15.8(0.3)	0.34(0.02)
PER	34.4 (0.7)	0.07(0.001)	41.7(0.1)	0.08(0.001)
GASmed	29.3(0.2)	0.40(0.01)	37.8(0.2)	0.13(0.01)
GASlat	31.8(1.3)	0.25(0.02)	41.7(0.1)	0.10(0.001)

IV. Discussion

We proposed a framework for coupling neural features to force-generation processes of human movement. This is realized by sampling statistical distributions of MUs and mapping them into MU-specific twitch responses.

Results of the statistical sampling showed bimodal distributions across all muscles. This bimodal nature may represent two populations of motor neurons (slow and fast) with overlapping neural features. We employed this characteristic to link neural features with contractile properties of the activation dynamics.

The estimated activation profiles showed high coefficients of determination (>0.8) for both models (Fig.4). Fig. 3, for example, depicts a high correlation between torque and its respective activation profile even with a very inconsistent (hesitant) movement. Although both models demonstrated robust estimations of activation profiles, Fuglevand's was substantially superior in computation time (~150 times faster). This was due to the possibility of discretizing this system instead of summing the contribution of individual twitches. Even though Raikova's model could provide better

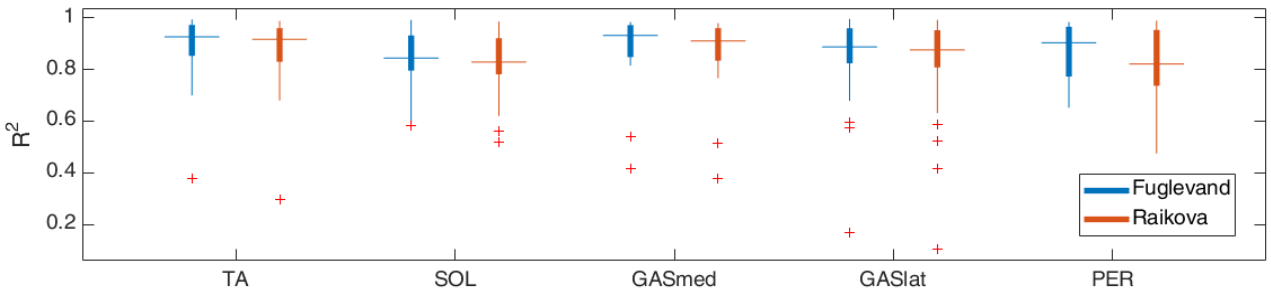

Figure 4. Square of the Pearson correlation coefficient between the reference torque and activation profiles derived from two twitch models: Fuglevand et al. [14] in blue and Raikova et al. [13] in red. This metric was computed for 5 different muscles: tibialis anterior (TA), soleus (SOL), medial and lateral gastrocnemius (GASmed and GASlat), and peroneus tertius (PER).

coefficients of determination with optimal values of half relaxation time, its computation time hinders potential applications to real-time scenarios.

The mapping of the half relaxation time and peak twitch amplitude will be addressed in future work, *i.e.*, we will build causal relations between the measured neural features and these contractile parameters, considering their unimodal distributions [16], [17]. Furthermore, an optimization of the distributions of these parameters is needed to better tailor the resulting models to an individual. This can be achieved by adjusting the means and standard deviations of the fitted Gaussian curves.

Importantly, the decomposition algorithm [12] limited the estimation of high-activation profiles. For instance, most of the outliers in Fig. 4 occurred during high-torque trials. This is due to the inability of decomposing smaller MUs (with low action potentials) in presence of bigger MUs (with higher action potentials). As the small MUs (slow) are the first to be recruited, long silent periods were common at the beginning of the ramps to 70% and 90% of the MVC.

Moreover, future work will implement a longitudinal tracking of MUs [18] to prevent possible repetitions within the sampling of neural features. This may offer a more precise picture of the projected features, and thus, a better neural mapping to activation dynamics.

V. Conclusions

We demonstrated a series of techniques for sampling MUs *in vivo*, displaying their statical organization and linking them to force-generation processes of human movement. Despite lacking optimization, our methodology provided solid activation profiles with a high degree of similarity to reference torques. After incorporating musculoskeletal modelling, this will enable closing the loop between the patient and neurorehabilitation devices, thereby addressing current limitations to customize neuromodulation strategies.

References

[1] A. A. M. Tax, J. J. Denier Van Der Gon, and C. J. Erkelens, "Differences in coordination of elbow flexor muscles in force tasks and in movement tasks," Springer-Verlag, 1990.

[2] T. S. Buchanan and D. G. Lloyd, "Muscle activity is different for humans performing static tasks which require force control and position control," *Neurosci. Lett.*, vol. 194, no. 1–2, pp. 61–64, Jul. 1995.

[3] S. J. De Serres and T. E. Milner, "Exp Brain Res (1991) 86:451~458 Wrist muscle activation patterns and stiffness associated with stable and unstable mechanical loads."

[4] L. A. Elias, R. N. Watanabe, and A. F. Kohn, "Spinal Mechanisms May Provide a Combination of Intermittent and Continuous Control of Human Posture: Predictions from a Biologically Based Neuromusculoskeletal Model," *PLoS Comput. Biol.*, vol. 10, no. 11, 2014.

[5] C. Pizzolato *et al.*, "Neuromusculoskeletal modeling-based prostheses for recovery after spinal cord injury," *Front. Neurorobot.*, vol. 13, p. 97, Dec. 2019.

[6] C. Pizzolato *et al.*, "CEINMS: A toolbox to investigate the influence of different neural control solutions on the prediction of muscle excitation and joint moments during dynamic motor tasks," *J. Biomech.*, vol. 48, no. 14, pp. 3929–3936, Nov. 2015.

[7] M. Sartori, D. G. Llyod, and D. Farina, "Neural Data-Driven Musculoskeletal Modeling for Personalized Neurorehabilitation Technologies," *IEEE Trans. Biomed. Eng.*, vol. 63, no. 5, pp. 879–893, May 2016.

[8] A. Holobar, V. Glaser, J. A. Gallego, J. L. Dideriksen, and D. Farina, "Non-invasive characterization of motor unit behaviour in pathological tremor," *J. Neural Eng.*, vol. 9, no. 5, 2012.

[9] I. Campanini, A. Merlo, and D. Farina, "Motor unit discharge pattern and conduction velocity in patients with upper motor neuron syndrome," *J. Electromyogr. Kinesiol.*, vol. 19, no. 1, pp. 22–29, 2009.

[10] A. Gogeascoechea *et al.*, "Interfacing With Alpha Motor Neurons in Spinal Cord Injury Patients Receiving Trans-spinal Electrical Stimulation," *Front. Neurol.*, vol. 11, p. 493, Jun. 2020.

[11] M. Sartori, U. Yavuz, and D. Farina, "In Vivo Neuromechanics: Decoding Causal Motor Neuron Behavior with Resulting Musculoskeletal Function," *Sci. Rep.*, vol. 7, no. 1, p. 13465, Dec. 2017.

[12] A. Holobar and D. Zazula, "Gradient Convolution Kernel Compensation Applied to Surface Electromyograms," *Indep. Compon. Anal. Signal Sep.*, pp. 617–624, 2007.

[13] R. T. Raikova and H. Ts Aladjov, "Hierarchical genetic algorithm versus static optimization-investigation of elbow flexion and extension movements," 2002.

[14] A. J. Fuglevand, D. A. Winter, and A. E. Patla, "Models of recruitment and rate coding organization in motor-unit pools," *J. Neurophysiol.*, vol. 70, no. 6, pp. 2470–2488, 1993.

[15] R. R. L. Cisi and A. F. Kohn, "Simulation system of spinal cord motor nuclei and associated nerves and muscles, in a Web-based architecture," *J. Comput. Neurosci.*, vol. 25, no. 3, pp. 520–542, Dec. 2008.

[16] R. A. Garnett, M. J. O'Donovan, J. A. Stephens, and A. Taylor, "Motor unit organization of human medial gastrocnemius.," *J. Physiol.*, vol. 287, no. 1, pp. 33–43, Feb. 1979.

[17] B. Steen Andreassen and L. Arendt-Nielsen, "Muscle Fibre Conduction Velocity In Motor Units Of The Human Anterior Tibial Muscle: A New Size Principle Parameter," 1987.

[18] E. Martinez-Valdes, F. Negro, C. M. Laine, D. Falla, F. Mayer, and D. Farina, "Tracking motor units longitudinally across experimental sessions with high-density surface electromyography," *J. Physiol.*, vol. 595, no. 5, pp. 1479–1496, 2017.